Korean J. Chem. Eng., **24**(6), 942-946 (2007)

Simulation of reactive precipitation processes using the network-of-zones model

Bahman ZareNezhad†

Chemical and Petroleum Engineering Department, Shiraz University of Technology,
P.O. Box 71555-313, Modarres Blvd., Shiraz, Iran
(*Received 29 October 2006 • accepted 12 April 2007*)

Abstract−A 2-D network-of-zones model is extended and applied to a reactive precipitation process in batch mode. The simulations are performed for a network of size 2×(10×10) for an elementary reaction through the solution of 1400 ODEs. The complicated interactions between mixing efficacy and the system kinetics are systematically investigated. When the stirrer speed is very slow, the crystal size distribution (CSD) of the product in the precipitator is determined by the intensity of mixing. Conversely, at higher stirrer speed, the CSD is controlled by the system kinetics. More effective mixing leads to an increase in the number of crystals, a reduction of the average size and a narrower crystal size distribution. The extended network-of-zones model presented in this work can be used conveniently for integrating computational fluid dynamics and reactive precipitation processes.

Key words: Reaction, Precipitation, Mixing, Simulation, CSD

INTRODUCTION

Although it is well known that mixing plays an important role in precipitation processes, there is still lack of detailed information about the interplay between the kinetics of the precipitation processes and the fluid dynamics of mixing. Previous work in this area has used empirical micro- or macro-mixing models [1,2] which do not in general reflect the details of the mixing and precipitation processes inside the vessel.

Traditionally, the design methodology of a plant precipitation process and its scale-up was a result of combining limited experimental data with empirical model predictions, sometimes based upon the ideal mixed suspension mixed product removal (MSMPR) crystallizer size distribution modeling. Using such an empirical approach, designers regularly failed to identify the optimum operating conditions or the optimum configuration of equipment, even when employing an experimental strategy to study every plausible case. Such a strategy was further hindered by lack of financial resources and time.

In this work, the 'network-of-zones' mixing model originally developed for description of turbulent mixing of fluid phases [3] is extended to study the effect of mixing on precipitation process in a batch stirred vessel. Although previous applications of the network-of-zones model has been done successfully in liquid-solid systems without chemical reaction [4,5], the system would be totally different when considering precipitation processes. The works of Brucato et al. only consider the suspension of mono size particles in solution phase. Precipitation not only involves chemical reaction but is also accompanied by crystal nucleation and growth so that the modeling description is more complicated.

PROCESS DESCRIPTION

In this work, the 2-D network-of-zones model is extended and applied to a batch reactive precipitation process. The vessel is subdivided into a total of 2×(N×N) zones such that 200 zones results for N=10. There are reaction species in each of these 200 perfectly mixed zones. Two species, A and B, are assumed to react together homogeneously with first order reaction kinetics with respect to each of the reacting components such that:

$$A+B\rightarrow C \tag{1}$$

$$r_C=k_R c_A c_B \tag{2}$$

Precipitation of the solid product C resulting from the liquid phase reaction occurs simultaneously because the fluid phase becomes supersaturated with respect to component C. Conventional power law equations of the form [6]:

$$J=k_b\Delta c_C^b=k_b(c_c-c_c^*)^b \tag{3}$$

$$G=k_g\Delta c_c^g=k_g(c_c-c_c^*)^g \tag{4}$$

are used to represent the nucleation and crystal growth kinetics, respectively.

In the (i, j) cell the species balance for the reactants can be described by:

$$\frac{dc_{I_{i,j}}}{dt}=\frac{q}{V_{i,j}}[c_{I_{i-1,j}}+\beta(c_{I_{i,j-1}}+c_{I_{i,j+1}})-(1-2\beta)c_{I_{i,j}}]-k_R c_{A_{i,j}} c_{B_{i,j}} \tag{5}$$

with $q=Q/n_c$, where Q is the total internal flow rate generated by the impeller, n_c is an even number for a 2×(N×N) network configuration and β (=0.2 for mixer volume and =1 on the impeller plane) is the turbulent lateral exchange parameter [7]. For the two reaction species, I=A or B and a 2×(10×10) network produces a set of 400 ordinary differential first order equations.

The mass balance for the product dissolved in solution is given by:

$$\frac{dc_{c_{i,j}}}{dt}=\frac{q}{V_{i,j}}[c_{I_{i-1,j}}+\beta(c_{c_{i,j-1}}+c_{c_{i,j+1}})-(1+2\beta)c_{c_{i,j}}] + k_R c_{A_{i,j}} c_{B_{i,j}}-3\frac{k_v\rho_c}{M_c}G_{i,j}m_{2_{i,j}} \tag{6}$$

†To whom correspondence should be addressed.
E-mail: zarenezhad@yahoo.com

In order to describe the crystal phase in the fluid field with the assumptions of negligible agglomeration and breakage, the moment transformations of the population balance equation can be employed in the network-of-zones model as species specific concentrations, i.e., number concentration, surface area concentration and mass concentration transport equations:

$$\frac{dm_{k_{i,j}}}{dt} = \frac{q}{V_{i,j}}[m_{k_{i-1,j}} + \beta(m_{k_{i,j-1}} + m_{k_{i,j+1}}) - (1+2\beta)m_{k_{i,j}}] + 0^k \cdot J_{i,j} - kG_{i,j}m_{k-1_{i,j}} \quad (7)$$

where k=0, 1, 2, 3.

To summarize, there are 7 ODEs in each zone; for a 2×(10×10) network 1400 ordinary differential equations must be solved simultaneously.

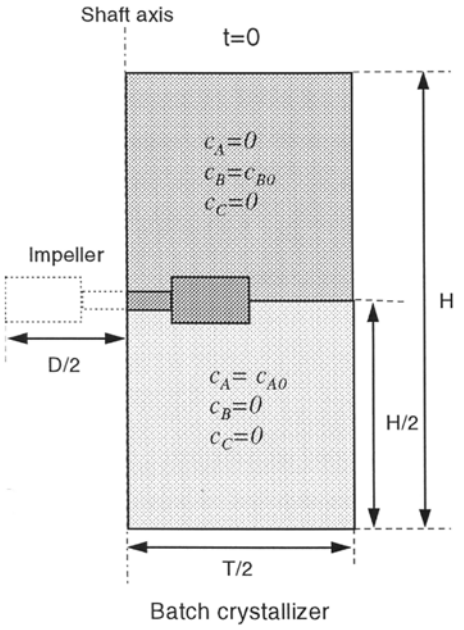

Fig. 1. The configuration and initial conditions of the batch crystallizer used in this study.

INITIAL CONDITIONS

It is very difficult to determine the initial state in a batch precipitation, as the distribution of each reactant cannot be clearly located at the beginning of the operation. We here assume that the two reactant solutions are separated absolutely at the start of the process (t=0). Species A is all in the lower half of the vessel below the impeller. The location of species B is in the upper half of the tank (see Fig. 2). The impeller is located at the centre of the crystallizer. Although this assumption is obviously idealized, it will be effective for investigating some aspects of the role of mixing in a batch precipitator.

Table 1. Parameters used in the simulation

c_{A0}	(kmol/m^3)	1.0
c_{B0}	(kmol/m^3)	1.0
c_{C0}	(kmol/m^3)	0.0
c_C^*	(kmol/m^3)	0.1
T	(m)	0.4
H	(m)	0.4
D	(m)	0.1
H_C	(m)	0.2
M_c	(kg/kmol)	200
ρ_c	(kg/m^3)	2000
k_a		3.68
k_b	no s^{-1}m^{-3} (kmol/m^3)$^{-4.5}$	7.5×10^7
k_g	m s^{-1} (kmol/m^3)$^{-1.5}$	5.0×10^{-8}
k_v		0.52
b		4.5
g		1.5
b		0.2
β'		1.0

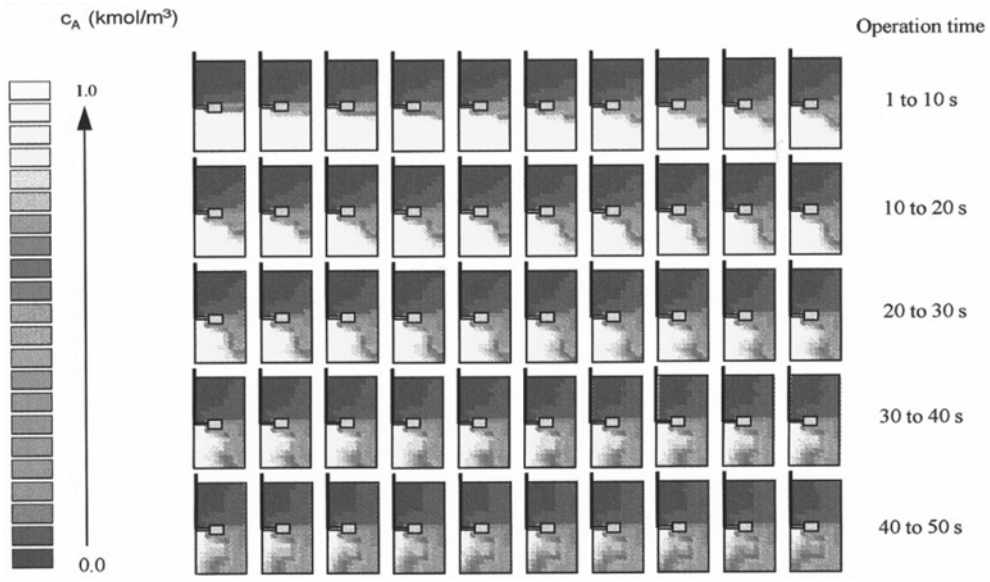

Fig. 2. Variation of the concentration of reactant A in the crystallizer (Initially A is only in the bottom half of the vessel).

In order to calculate the perfect mixing case, the composition of all cells in the tank is assumed to be equal at any given time. The initial condition for this case assumes that the composition of every cell is $c_A=c_{Ao}/2$ and $c_B=c_{Bo}/2$. The specific parameters used in the simulation are listed in Table 1 [8]. These parameter values are typical of a reactive precipitation system having high nucleation and growth rates. The integration time step of one second is used so as to guarantee convergence but also to achieve a reasonable computation time.

RESULTS AND DISCUSSION

The development of the concentration of the different species in each zone needs to be visualized so that the results of simulations can be directly investigated and the interplay of precipitation process can be explored in an understandable way. A 2-D image has been achieved by use of advanced graphic package.

Fig. 2 shows how the concentration of reactant A varies with operating time over the first 50 seconds and how its distribution in the whole vessel is controlled by both mixing and reaction. Reactant A is initially only in the bottom half of the vessel. When it enters the upper part of the vessel within the flow loop produced by the impeller, component A disappears immediately as a result of the high reaction rate because the concentration of B is very high in the upper region. Below the impeller the concentration of A is reduced with mixing transfer and reaction due to B entering the lower region. The position of the streamlines can be clearly imagined through the distribution of the concentration of A, which has the appearance of a whirlpool around the centre position. The centre of the whirlpool is always the region of high concentration because exchange between the loops is weak relative to that in the main flow loop. The variation of reactant B is the mirror image of that of A. Note that there is no turbulent exchange between the cells immediately

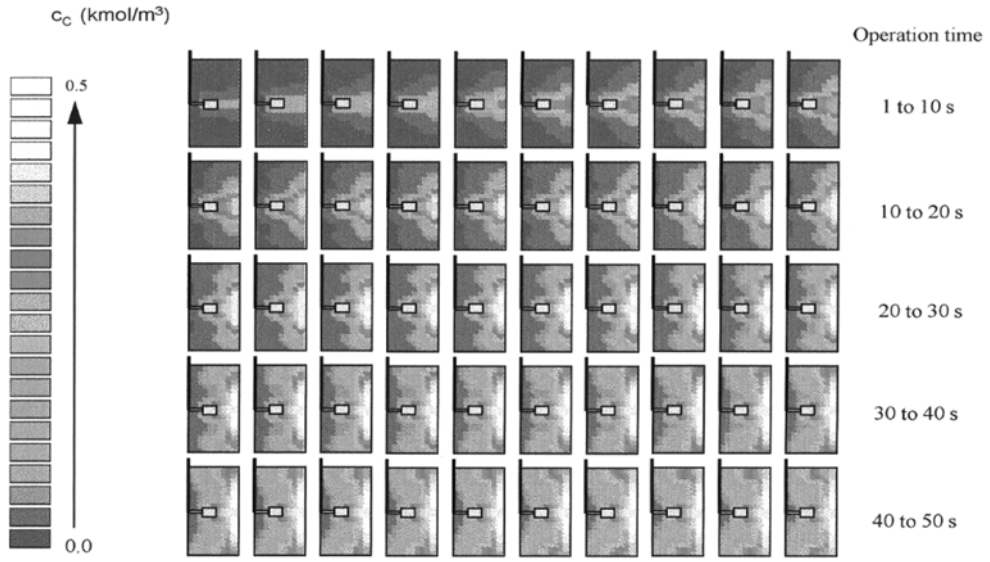

Fig. 3. Variation of the concentration of product C in solution in the crystallizer.

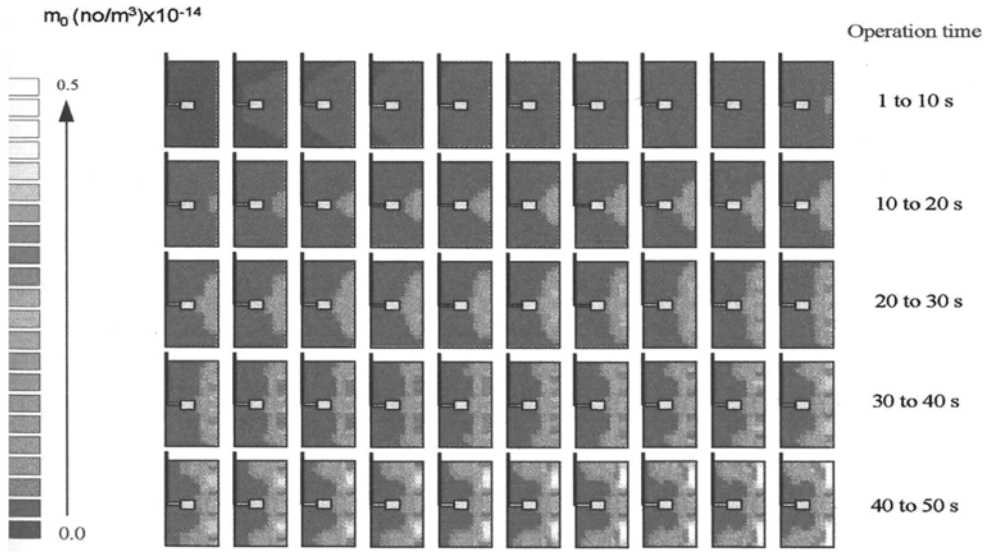

Fig. 4. Variation of the crystal number concentration in the crystallizer.

above and below the impeller, which is why the concentration of A or B is always higher at these regions. After 50 seconds the distribution of reactant becomes uniform throughout the vessel.

The distribution of concentration of product C in solution phase is represented in Fig. 3. Product C appears first at the border of the upper and lower parts where both A and B are present at high concentration with intense turbulent mixing. It then spreads progressively following the main flow and turbulent diffusion. Once the concentration of C exceeds the saturation concentration, in some zones, nucleation occurs immediately and continuously in these places. Meanwhile nuclei grow under the action of supersaturation and all particles move with the liquid phase. Product C in the solution phase is thus consumed by nucleation and growth rates. This is a very complicated feedback process in which the solid and liquid phases influence each other. Fig. 4 represents the dynamic distribution of the zeroth moment, which represents total particle number per unit volume. The variation of the third moment representing the magma density is described in Fig. 5. Comparing Figs. 3-5, it can be seen that there is a time displacement for the appearance of the maximum of each concentration at a particular point, which probably results from the feedback action mentioned above.

From these graphics we can conclude that the crucial stage for the influence of mixing on batch precipitation is at the beginning of the operation and this will determine in large part the final crystal size distribution in the precipitator.

Effect of mixing on CSD is demonstrated quantitatively in Fig. 6. First, Fig. 6 shows that the mass-average size of the product crystals varies with total impeller flow rate. The reduction of the average size due to more effective mixing is directly related to the increase in crystal numbers. As shown in Fig. 6, the coefficient of variation (C.V) of the product particles is reduced when mixing becomes more effective. If the value of C.V is smaller, the crystals are distributed within a narrower size range. Variation of the zeroth moment and hence the crystal number concentration with total flow rate is also represented in Fig. 6. The number of crystals increases rapidly with increasing value of Q, particularly in the poor mixing region.

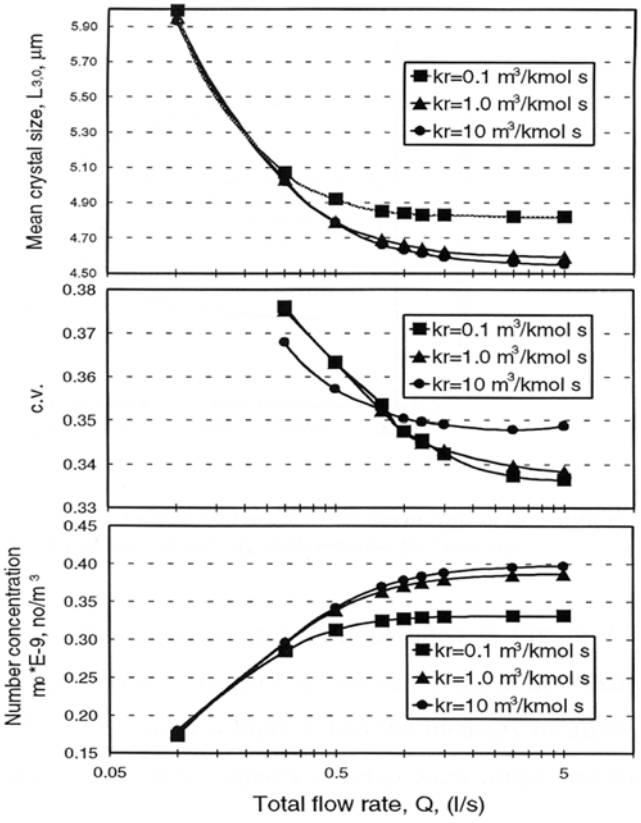

Fig. 6. The influence of stirring intensity and reaction rate constant on the properties of the precipitated product.

The influence of reaction kinetics on the system is also demonstrated in Fig. 6. Each figure includes three curves representing different reaction rate constants. Mixing is more important when the reaction rate constant is high. When the intensity of mixing is low so that the mixing is ineffective, the three curves overlap each other and the precipitation process is controlled by the intensity of mixing. As the mixing becomes effective enough, the curves separate

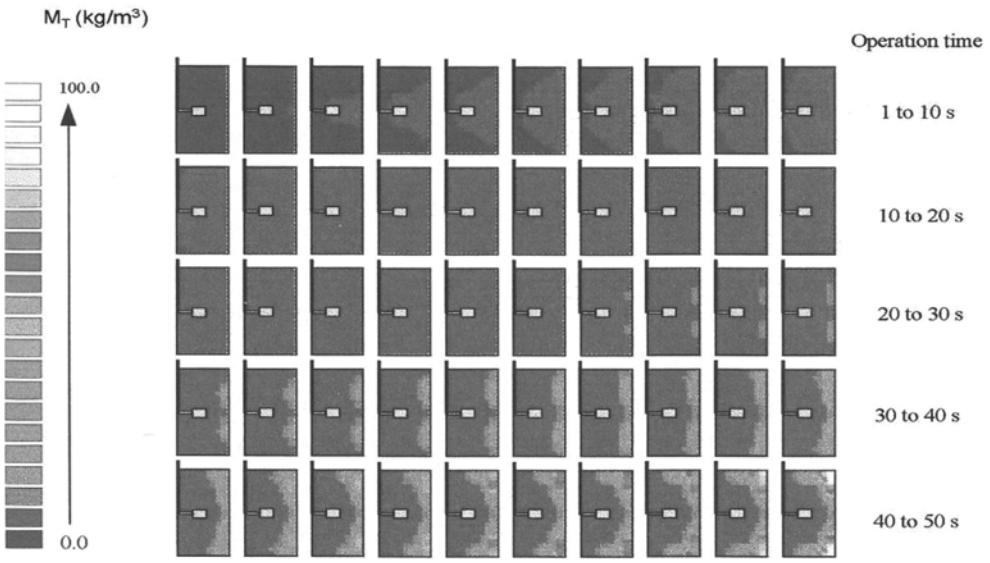

Fig. 5. Variation of the magma density in the crystallizer.

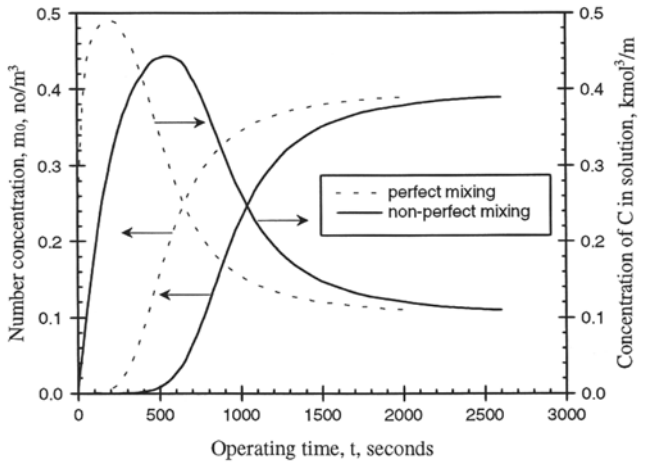

Fig. 7. Variation of the number concentration and product C concentration in solution with operation time: comparison of perfect mixing with non-perfect mixing.

and reach the limit corresponding to the perfect mixing case. In this situation the system is controlled by the system kinetics. Systems having high kinetic constants may be controlled by mixing, but when the reaction is fast enough, increasing the reaction rate constant has less effect on the system as can be seen by comparing the curves at 1 and 10 $m^3\ kmol^{-1}s^{-1}$ in Fig. 6.

Effect of mixing can be explained with the aid of Fig. 7, which represents a comparison of perfect mixing and the non-perfect mixing. The different concentrations in Fig. 7 are the mean values based on the total working solvent volume in the crystallizer. The curve for concentrations of C in the perfect mixing case shows a sharp narrow peak, while the zero moment curve rises very steeply. This means that most of the particles in the perfect mixing case are produced at the beginning of the operation over a short period of time because of the uniform high supersaturation at this stage of the process. All these particles then grow for a similar time period till the end of the operation so that the sizes of all the crystals are distributed over a comparatively narrow range. Since a large number of crystals are produced at the beginning and the supersaturation is consumed rapidly, the crystals do not grow very large. On the other hand, in the non-perfect mixing case the distribution of supersaturation is not uniform. In some places it is very high and some particles appear early in such regions and thereby have a longer growth period and higher growth rates. The growth of these particles consumes supersaturation so that the nucleation rate decreases, which results in a smaller number of crystals and a wider size distribution.

CONCLUSIONS

The network-of-zones model forms a computationally convenient framework for calculating the effect of departures from perfect backmixing and was successfully applied to describe the role of mixing in a precipitation process. The complicated interactions between mixing efficacy and the system kinetics were systematically investigated. When the stirrer speed is very slow, the crystal size distribution (CSD) of the product in the precipitator is determined by the intensity of mixing. Conversely, at higher stirrer speed, the CSD is controlled by the system kinetics. More effective mixing leads to an increase in the number of crystals, a reduction of the average size and a narrower crystal size distribution. The presented extended network-of-zones model can be used as a simple CFD technique for integrating the hydrodynamics and precipitation processes. The results of this application reveal the interplay of mixing and precipitation and exhibit the role of mixing in precipitation processes.

NOMENCLATURE

c_A : molar concentration of component A [$kmol/m^3$]
c_B : molar concentration of component B [$kmol/m^3$]
c_C : molar concentration of component C [$kmol/m^3$]
c_I : concentration of component I (A or B)
k_R : reaction rate constant [$m^3/kmol \cdot s$]
k_b : nucleation rate constant [$no/(sm^3(kmol/m^3)^b)$]
k_g : growth rate constant [$m/s(kmol/m^3)^g$]
k_v : shape factor
r_c : rate of production of component C [$kmol/sm^3$]
J : nucleation rate [no/m^3s]
G : Growth rate [m/s]
c_c^* : saturation concentration [$kmol/m^3$]
Δc_c : supersaturation [$kmol/m^3$]
b : nucleation order
g : growth order
q : flow in circulation loop [m^3/s]
Q : volumetric pumping capacity of the impeller [m^3/s]
$V_{i,j}$: cell volume [m^3]
ρ_c : crystal density [kg/m^3]
M_c : molecular weight [kg/kmol]
m_2 : second moment of CSD [$no \cdot m^2/m^3$]
m_k : k^{th} moment of CSD [$no \cdot m^k/m^3$]
CV : coefficient of variations=$(m_0 m_2/m_1^2 - 1)^{1/2}$
t : time variable [s]
i, j : cell index

Greek Letters

β : lateral exchange flow coefficient
β' : lateral exchange flow coefficient in the impeller region

REFERENCES

1. N. S. Tavare, *AIChE J.*, **41**, 2537 (1995).
2. J. Baldyga, J. R. Bourne and S. J. Hearn, *Chem. Eng. Sci.*, **52**, 457 (1997).
3. P. Knysh and R. Mann, *IChemE Symp. Ser.*, **89**, 127 (1984).
4. A. Brucato and L. Rizzutti, Proceedings, 6th Euro. Conf. on Mixing, Pavia, 273(1988).
5. A. Brucato, F. Magelli, M. Nocentini and L. Rizzutti, *Trans IChemE*, **69**, 43 (1990).
6. A. D. Randolph and M. A. Larson, *Theory of particulate processes*, Academic Press, 2nd ed., New York (1988).
7. R. Mann, P. Ying and R. B. Edwards, Proceedings, 8th Euro. Conf. on Mixing, 317 (1994).
8. N. S. Tavare and J. Garside, *Trans. IChemE*, **68**, 115 (1990).